An ODE-based swift and dynamic sewer airflow model

Shi, Tao; Li, Jiuling; Ge, Jingyu; Watts, Shane; Wang, Yaran; Sharma, Keshab; Yuan, Zhiguo

Published in:
Water Research

Published: 01/04/2025

Document Version:
Final Published version, also known as Publisher's PDF, Publisher's Final version or Version of Record

Published version (DOI):
10.1016/j.watres.2024.123083

Publication details:
Shi, T., Li, J., Ge, J., Watts, S., Wang, Y., Sharma, K., & Yuan, Z. (2025). An ODE-based swift and dynamic sewer airflow model. *Water Research*, *273*, Article 123083. https://doi.org/10.1016/j.watres.2024.123083

Water Research 273 (2025) 123083

Contents lists available at ScienceDirect

Water Research

journal homepage: www.elsevier.com/locate/watres

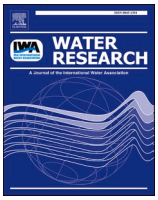

An ODE-based swift and dynamic sewer airflow model

Tao Shi [a], Jiuling Li [a], Jingyu Ge [a], Shane Watts [a], Yaran Wang [b,c], Keshab Sharma [a], Zhiguo Yuan [d,e,*]

[a] Australian Centre for Water and Environmental Biotechnology (formerly AWMC), The University of Queensland, St. Lucia, Brisbane 4072, QLD, Australia
[b] School of Environmental Science and Engineering, Tianjin University, Tianjin 300350, PR China
[c] Key Laboratory of Efficient Utilization of Low and Medium Grade Energy, MOE, Tianjin University, Tianjin 300350, PR China
[d] School of Energy and Environment, City University of Hong Kong, Hong Kong SAR, China
[e] State Key Laboratory of Marine Pollution, City University of Hong Kong, Hong Kong SAR, China

ARTICLE INFO

Keywords:
Airflow model
Digital twins
Sewer
Navier-stokes equations
Corrosion
Odour

ABSTRACT

Airflow models are powerful tools for ventilation design to achieve odour and corrosion mitigation in sewer networks. Currently, there lacks a model able to efficiently predict in-sewer dynamic airflows, as all available dynamic models with an acceptable accuracy are computationally demanding. In this study, a swift dynamic airflow model based on an ordinary differential equation (ODE) is derived by simplifying the one-dimensional Navier Stokes Equations (NSE), supported by the observation that the NSE solutions always display negligible spatial variations in air velocity when applied to a sewer conduit. The ODE model reproduces the NSE airflow predictions with a high-level fidelity, with time consumption reduced by two orders of magnitude. The ODE model was calibrated and validated using comprehensive datasets collected from a pilot sewer. The calibrated ODE model was applied to simulated sewer networks in both natural and forced ventilation scenarios, which demonstrates the accuracy, robustness, and efficiency of the model. The swift dynamic airflow model will provide strong support to effective sewer ventilation design for odour and corrosion management in sewers.

1. Introduction

Sewer corrosion and odour induced by hydrogen sulfide (H_2S) costs billions of dollars annually worldwide (Jiang et al., 2015; Song et al., 2020). The problems are caused by a sequence of reactions/processes of: (1) H_2S production by sulfate-reducing bacteria (SRB) in the anaerobic environment; (2) H_2S release from wastewater to sewer headspace, and its further diffusion into the liquid film on unsubmerged sewer wall; (3) sulfuric acid production by sulfide-oxidizing bacteria (SOB) in the liquid film, and (4) destructive reactions of sulfuric acid and concrete materials. Multiple techniques have been applied for odour and corrosion management in sewers, including ventilation, chemical dosing, and the use of corrosion resistant materials for lining or coating (Liang et al., 2024; Jiang et al., 2015; Matos et al., 2019; Song et al., 2021; Zhang et al., 2023; Zuo et al., 2024).

Ventilation, defined as the introduction of fresh atmospheric air and removal of stale gases from sewers (Corsi et al., 1989; Edwini-Bonsu, 2006b; Pomeroy, 1945; Qian et al., 2021; Studley, 1939), is an effective and powerful solution if appropriately designed and operated (Brown, 1937; Donaldson, 1932; H., 1965; Matos et al., 2019, 2020; Pomeroy and Bowlus, 1946; Vollertsen et al., 2008). Ventilation reduces the moisture and H_2S levels in sewer air thus mitigating sewer corrosion (Matos et al., 2020; Bu et al., 2021; Jiang et al., 2017, 2015). The controlled release of the malodorous in-sewer gas, including gas treatment, eliminates/reduces the odour nuisance to residents (Bu et al., 2021).

Despite its wide application, ventilation is normally designed based on rules of thumb (Hurse and Ochre, 2008; Matos et al., 2020). One design parameter for sewer ventilation is the sewer-air renewal rates (Matos et al., 2020). Some early engineering experiences indicate that 5 times renewal per hour is adequate for corrosion prevention (Thistlethwayte, 1972). However, this empirical design is not always effective or cost-efficient. The sewer corrosion rate is jointly determined by the H_2S, relative humidity and temperature levels in sewer air, and the sewer wall temperature (Joseph et al., 2012). All these variables are dynamic, influenced by factors such as the in-sewer hydraulics, the atmospheric temperature and humidity, and the wastewater temperature, along with the airflow rate. Therefore, the optimal airflow rate is expected to be dynamic, with optimal design to be supported by dynamic

* Corresponding author
E-mail addresses: uqtshi@uq.edu.au (T. Shi), jiuling.li@uq.edu.au (J. Li), jingyu.ge@uq.edu.au (J. Ge), s.watts@uq.edu.au (S. Watts), yaran_wang@tju.edu.cn (Y. Wang), k.sharma@uq.edu.au (K. Sharma), zhigyuan@cityu.edu.hk (Z. Yuan).

https://doi.org/10.1016/j.watres.2024.123083
Received 2 August 2024; Received in revised form 27 December 2024; Accepted 30 December 2024
Available online 31 December 2024

Nomenclature

ρ	air density (kg/m^3)
p	air pressure (pa)
A	area of headspace in a sewer cross-section (m^2)
U	mean longitudinal air velocity (m/s)
U_w	averaged water velocity in a sewer cross-section (m/s)
t	time (s)
x	distance in longitudinal direction (m)
Δx	step size used to discretise Eq. (3) and Eq. (4) (m)
z	elevation of the invert (m)
μ	viscosity of air (kg/(m·s))
g	gravitational acceleration (m/s^2)
B	the surface width of water flow (m)
P	the perimeter of the unwetted pipe (m)
C_d	the water drag coefficient
f	the pipe friction coefficient
K	the reciprocal of molar mass of air (34.53 mol/kg)
R	the ideal gas constant (8.314 J/(K·mol))
T	temperature of sewer air (K)
p_0	the air pressure at the start of a pipe (pa)
p_N	the air pressure at the end of a pipe (pa)
L	length of a sewer pipe (m)
S	slope of a sewer pipe
Δp	the air pressure difference between the two ends of a sewer pipe (pa)
R_h	the hydraulic radius
S_f	the hydraulic slope

sewer airflow models.

The theoretical basis for mechanistic airflow models for sewer pipes has been well established. The Navier-Stokes Equations (NSE), a set of partial differential equations (PDEs), are widely used to describe the conservation of mass and momentum for viscous fluid. Lack of analytical solutions, the NSE need be numerically solved, which is computationally demanding and time-consuming. Simplifications, with various assumptions, are usually needed to reduce the computational complexity (Edwini-Bonsu, 2006b; Qian et al., 2018; Zhang et al., 2020; Zobeyer et al., 2020) (Table S1 in part S1 of SI). The simplified models often lose their dynamic nature (i.e., becoming steady-state models) or accuracies, with solutions significantly different from predictions by the original NSE.

By assuming a fully developed and incompressible airflow under steady state conditions, Edwini-Bonsu (2006a) and Edwini-Bonsu and Steffler (2004) used the Reynolds-averaged NSE to investigate airflow velocities both parallel and perpendicular to the pipe. These studies revealed the velocity distributions in a cross-sectional area of a sewer pipe, which is useful to guide future modelling work. However, this three-dimensional (3D) model is generally too computationally demanding for network-wide airflow modelling, even under steady-state conditions. The one-dimensional (1D) model composed of momentum and continuity equations (Eqs. (1)-2) is an attractive alternative, which has been investigated in the recent decade. In Eq. (1), the five terms on the right side represent air pressure, viscosity, gravity, water drag, and pipe friction forces affecting air movement, respectively.

$$\frac{\partial \rho AU}{\partial t}+\frac{\partial \rho AU^2}{\partial x}=-A\frac{\partial p}{\partial x}+\frac{\partial \mu A\frac{\partial U}{\partial x}}{\partial x}-\rho Ag\frac{\partial z}{\partial x}+\frac{C_d}{2}\rho B(U_w-U)\cdot|U_w-U|-\frac{f}{8}\rho PU\cdot|U| \tag{1}$$

$$\frac{\partial(\rho A)}{\partial t}+\frac{\partial(\rho AU)}{\partial x}=0 \tag{2}$$

Wang et al. (2012) used these partial differential equations to simulate air pressure and velocity in a sewer network. A sewer pipe was discretised into multiple tanks, with the momentum and continuity equations solved for each tank with the Finite Volume Method, to obtain the spatiotemporal airflow characteristics. Given the computational complexity, the use of this model for large-scale sewer networks comprising hundreds to thousands of sewer pipes will prove challenging.

Ward et al. (2011) further simplified the 1D model by neglecting terms $\frac{\partial \rho AU}{\partial t}$, $\frac{\partial \rho AU^2}{\partial x}$, and $\frac{\partial \mu A\frac{\partial U}{\partial x}}{\partial x}$ in Eq. (1), thus obtaining a steady-state model for fully developed airflows (Table S1 in part S1 of SI). The simulation efficiency was dramatically improved in network-wide modelling (Qian et al., 2018; Zhang et al., 2020; Zobeyer et al., 2020), but the model is not suitable for predicting non-steady state or non-uniform airflows.

Various empirical airflow models have also been proposed, which calculate the longitudinal air velocity based on the wastewater velocity, with or without explicitly considering the impact of the width of the water-air interface on the water drags and the unwetted perimeter on the wall frictions (Edwini-Bonsu and Steffler, 2004; Lowe, 2017). These empirical equations are usually applicable to specific pipe conditions, and do not have a universal applicability (Qian et al., 2021). Correspondingly, most current simulations of corrosion-related key processes (heat, and humidity transfer) are based on empirical airflow models (Durrenmatt and Wanner, 2014; Figueroa et al., 2021), inducing potentially inaccurate assessment of corrosion rate.

The above literature review (see also Table S1 in SI) indicates that there lacks a sewer airflow model that is both efficient, thus applicable to large sewer networks, and general - able to predict dynamic airflows. This study aims to develop a 1D airflow model capable of predicting non-steady sewer airflows with a performance comparable to the 1D partial differential equations, but with much improved simulation efficiency. This is achieved by simplification with assumptions well supported by the solutions of the 1D partial differential equations. The simplified model (ODE-based) is then calibrated and validated using extensive data collected with specifically designed experiments on a pilot sewer. The performance of the model is then demonstrated via its application to sewer networks.

2. Deriving an ODE model from the full 1D NSE

We first transformed 1D NSE (Eq. (1) and Eq. (2)) into the following equivalent form, where the ideal Gas Law was applied to replace the air density with pressure ($\rho=\frac{p}{KRT}$):

$$\frac{\partial U}{\partial t}=-U\cdot\frac{\partial U}{\partial x}-\frac{KRT}{p}\cdot\frac{\partial p}{\partial x}+\frac{\mu KRT}{p}\cdot\frac{\partial^2 U}{\partial x^2}+\frac{\mu KRT}{pA}\cdot\frac{\partial U}{\partial x}\cdot\frac{\partial A}{\partial x}-g\cdot\frac{\partial z}{\partial x}+\frac{C_d}{2}\cdot(U_w-U)\cdot|U_w-U|\cdot\frac{B}{A}-\frac{f}{8}\cdot U\cdot|U|\cdot\frac{P}{A} \tag{3}$$

$$\frac{\partial p}{\partial t}=-\frac{p}{A}\frac{\partial A}{\partial t}-p\frac{\partial U}{\partial x}-\frac{pU}{A}\frac{\partial A}{\partial x}-U\frac{\partial p}{\partial x} \tag{4}$$

Eq. (3) and 4 were then discretised with respect to x with Finite Difference Method. The PDEs were thus transformed into a set of $2N$-1 ($N = L/\Delta x$) ordinary differential equations (ODEs), which were implemented in MATLAB for airflow simulation, along with the Saint-Venant equations for unsteady hydraulic simulations (Capart et al., 1997; Li et al., 2022). The hydraulic simulations provided variables A, P, $\frac{\partial A}{\partial t}$ and U_w to the airflow model as its inputs. Implementation details are shown in part S2 of SI. Simulations were performed in 52 scenarios with the

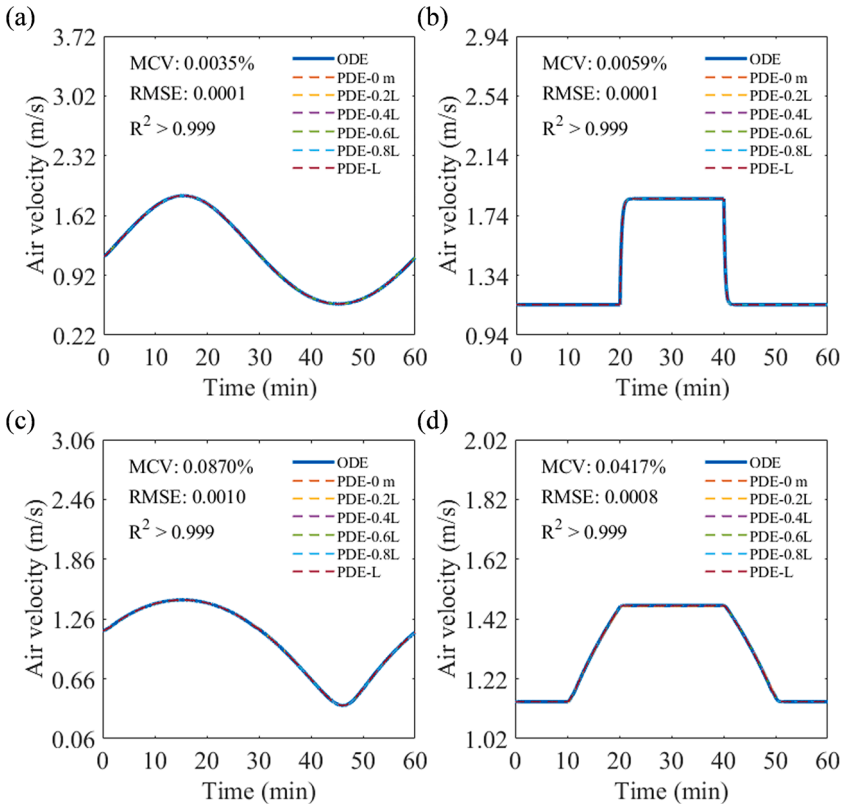

Fig. 1. The air velocities predicted by the full 1D NSE for locations 0, 0.2 L, 0.4 L, 0.6 L, 0.8 L, and 1 L, and by the simplified 1D ODE-based equation. The results with Parameter Setting 1 are shown in this figure as examples (see Figure S2 in SI for the complete set of figures). (a) Boundary condition 1; (b) Boundary condition 2; (c) Boundary condition 3; (d) Boundary condition 4. See Table S2 in SI for boundary condition definitions).

combination of 13 parameter settings and 4 boundary conditions. Details of simulation setting are shown in part S3 of SI.

The temporal velocity profiles predicted by the full discretised 1D NSE for multiple locations (0, 0.2 L, 0.4 L, 0.6 L, 0.8 L, and L) are shown in Fig. 1 and Figure S2 (part S4 of SI). For all 52 scenarios, the temporal velocity profiles at all locations are nearly identical, with the mean coefficient of variation (*MCV* – Eqs. S12, S13 in part S5 of SI) consistently lower than 0.3 %, despite the rapid changes in hydraulic or pressure boundary conditions in most cases. Besides, the full model successfully described the compressibility of air according to the pressure distribution along the pipe, displayed in Figure S3 (part S4 of SI).

The above observation provides an opportunity to simplify Eq. (1) by assuming $\frac{\partial U}{\partial x} = 0$ and $\frac{\partial^2 U}{\partial x^2} = 0$:

$$\frac{dU}{dt} = -\frac{KRT}{p}\cdot\frac{\partial p}{\partial x} - g\cdot\frac{\partial z}{\partial x} + \frac{C_d}{2}\cdot(U_w - U)\cdot|U_w - U|\cdot\frac{B}{A} - \frac{f}{8}\cdot U\cdot|U|\cdot\frac{P}{A} \tag{5}$$

Integrating Eq. (5) on both sides with respect to x yields Eq. (6), which is an ordinary differential equation (ODE) with U as the state variable. Eq. (6) is called the simplified, ODE-based airflow model hereafter.

$$\frac{dU}{dt} = -\frac{KRT}{L}\ ln(p_N / p_0) + gS + \frac{1}{L}\int_0^L \left[\frac{C_d}{2}\cdot(U_{w_{(x)}} - U)\cdot|U_{w_{(x)}} - U|\cdot\frac{B_{(x)}}{A_{(x)}} - \frac{f}{8}\cdot U\cdot|U|\cdot\frac{P_{(x)}}{A_{(x)}}\right]dx \tag{6}$$

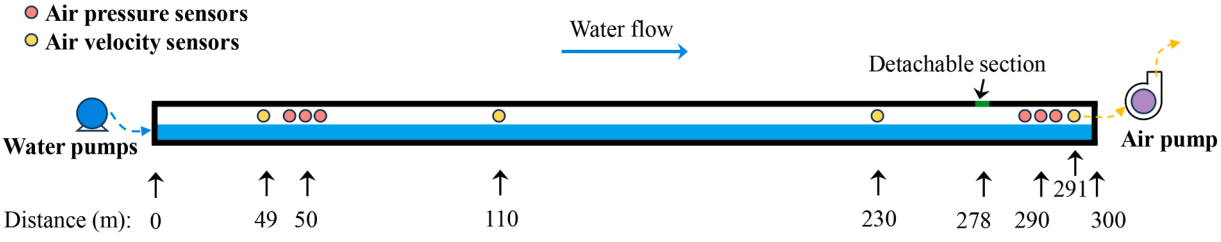

Fig. 2. The schematic of the pilot sewer.

Table 1
Summary of the pilot sewer experiments.

Set	Type	Objectives	Air pump (hp)	Water pump (L/min)	Measurements
1	Steady-state hydraulic experiments	Calibration of Manning's coefficient (n)	–	Constant at 142; 285; 405; 523; 665; 775, 952; 1074; 1245; 1365	Wetted perimeter of the pipe
2	Steady-state ventilation experiments	Calibration of the pipe friction (f) and water drag coefficient (C_d)	Constant at 0.6; 0.9; 1.2; 1.5; 1.6; 1.7; 1.8	For each air pump power, the water flow was controlled at 0; 285; 523; 775	Air pressure Air velocity Air temperature
3	Dynamic ventilation experiments	Validation of the simplified ODE-based airflow model	For each water flow, the air pump was continuously varied between 0.6 - 2 Step change to 0.6; 0.9; 1.2; 1.5; 1.6; 1.7; 1.8	Constant at 285; 523; 775 For each ventilation power level, the water flow was switched between 142 and 405 L/min	Air pressure Air velocity Air temperature

The ODE-based model (Eq. (6)) was subsequently applied to the same 52 simulation scenarios, with the results also displayed in Fig. 1 and Figure S2, for comparison with the full model. The Root Mean Squared Error and Coefficient of determination values (*RMSE* and R^2 – Eqs. S14, S15 in part S5 of SI) were calculated (Fig. 1 and Figure S2) based on the averaged air velocity from the full model and the ODE-based model results, showing a high-level fidelity of the ODE-based model.

3. Calibration, validation, and performance evaluation of the 1D ODE model

3.1. Pilot sewer experiments for model calibration and validation

The pilot sewer and the overall experimental plan. Hydraulic and ventilation experiments were conducted on a pilot gravity sewer pipe in the Luggage Point Wastewater Treatment Plant, Brisbane, Queensland, Australia, to collect data for the calibration and validation of the newly obtained ODE-based sewer airflow model. The PVC sewer pipe has a length of 300 m, an inner diameter of 0.238 m, and an average slope of 0.59 % (Figure S4 in part S6 of SI). The water flow rate was controlled with four water pumps. The ventilation was applied with one air pump. The air pressures were continuously measured at two locations, 50 and 290 m downstream of the water inlet, with three pressure sensors (Yocto-Meteo-V2, Yoctopuce) installed at each location to provide redundancy (Fig. 2). Air velocities were measured at four locations 49, 110, 230, and 291 m downstream of the water inlet, each with one velocity sensor (RK100–05, Ocean Controls) installed (Fig. 2). Online data were logged with a Yoctopuce signal acquisition system. The velocity sensors were moved vertically to obtain the averaged air velocity in the cross-section. The pipe had a detachable section 278 m from the water inlet (Fig. 2), which supported manual measurement of the water level/wetted perimeter (Figure S5 in part S7 of SI). Three types of experiments were conducted, as summarized in Table 1 and detailed below.

Steady state hydraulic experiments and calibration of parameter *n*. Hydraulic experiments were conducted to provide data for calibrating the Manning coefficient (n) of the pipe, a parameter in the Saint-Venant equations. The Saint-Venant equations were then solved to provide the water area (A_w) and water flow velocity (U_w) to the airflow model (Eq. (6)). The experiments were conducted with 10 different water flowrates. Once a steady state was reached, the wetted perimeter was measured five times with the average value used in the calculation of n. With the wetted perimeter, the water cross-section area and hydraulic radius were calculated based on the pipe geometry. The averaged water velocity was then calculated using the known flowrate of the water pumps (Part S7 in SI for details). Parameter n was then estimated, through nonlinear least squares optimisation, by fitting the following equation (Manning's equation) with the measured water velocity:

$$U_w = \frac{1}{n} R_h^{2/3} S_f^{1/2} \tag{7}$$

The Root Mean Squared Error (*RMSE*), Coefficient of Determination

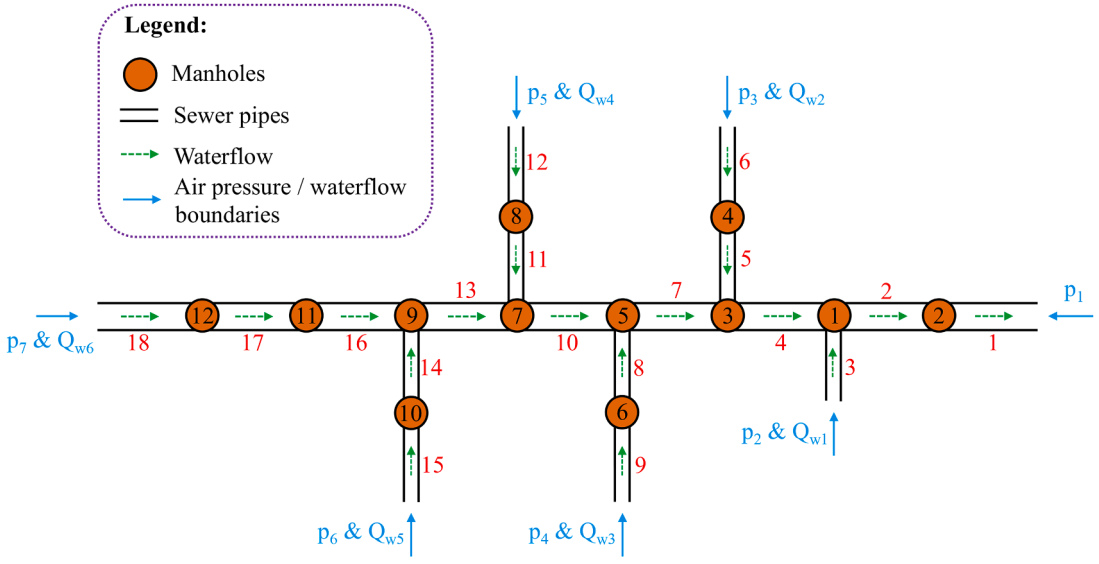

Fig. 3. The schematic of the simulated sewer network A. Pipe Sections 1, 2, 4, 7, 10, 13, 16, 17, 18 have a diameter of 1.35 m, and the rest have a diameter of 0.9 m. All pipe sections have a length of 100 m and a slope of 0.9 %. Access chambers on the main sewer line (1–3, 5, 7, 9, 11, 12) have a 1.8 m diameter, and the rest have a 1.2 m diameter. Mass balance equations for access chambers are shown in Part S9 of SI.

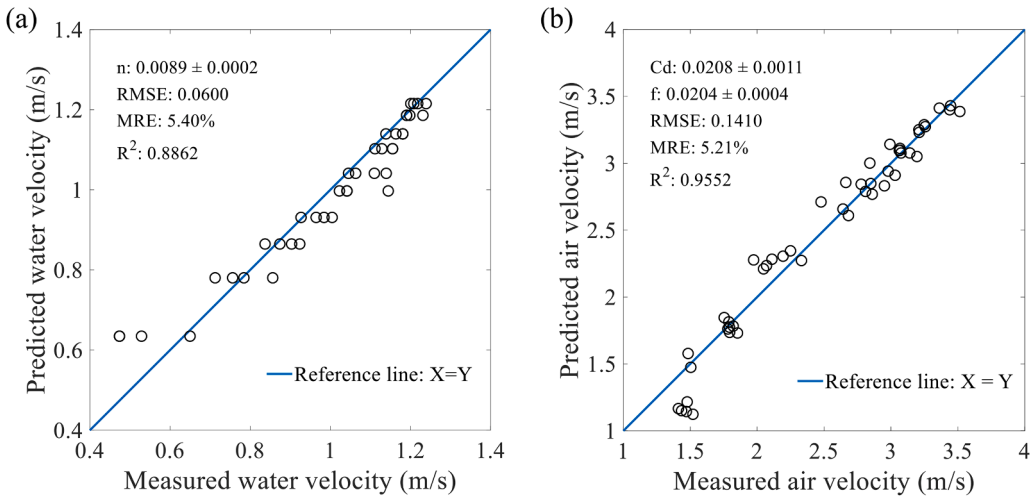

Fig. 4. The model-predicted and experimentally determined water velocities in the first set of experiments (a), and air velocities in the second set of experiments (b).

(R^2), and Mean Relative Error (*MRE*) were calculated to evaluate the fitting quality, as detailed in Part S5 in SI.

Steady state ventilation experiments and calibration of parameters C_d and f. Steady state ventilation experiments were conducted to provide data for calibrating the pipe friction coefficient (f) and the water drag coefficient (C_d) needed in the ODE-based model (Eq. (6)). Experiments were conducted with 7 different air pump power levels. All these pump power levels were above 0.6 Hp (Table 1) to minimise the impact of fluctuating wind pressure and maintain steady state conditions. At each power level, tests were first done without a water flow (repeated 4 times) and then at 3 different water flow rates, resulting in 49 tests in this set of experiments.

Each test lasted for about 25 min, during which the air velocity and pressure were continuously monitored with the online sensors. The biases of the pressure sensors, and the air pressure difference balanced with gravity were measured in the pretests (details are described in part S8 of SI). At the steady state, the height of all velocity sensors was adjusted to ¼, ½, and ¾ height of headspace below the pipe crown. The velocity variation among the locations within the same cross-section was not as significant as reported in literature for natural ventilation scenarios (Edwini-Bonsu, 2006a). The average cross-sectional air velocity monitored was approximately equal to the air velocity at half the headspace height. Wetted perimeters and water velocities were calculated with Manning's equation with the calibrated n mentioned before.

Based on data collected in the above experiments, the calibration was implemented according to the steady-state form of the ODE-based model (Eq. (8)). The C_d and f values were calibrated simultaneously with the linear least squares fitting method. The air velocity was calculated with Eq. (8), with the C_d and f values obtained, based on the measured air pressure. The *RMSE*, *MRE*, R^2 were calculated to evaluate the effectiveness of the air velocity prediction using the calibrated C_d and f values.

$$-KRT\cdot\frac{ln(p_N/p_0)}{L}+gs+\frac{C_d}{2}\cdot(U_w-U)\cdot|U_w-U|\cdot\frac{B}{A}-\frac{f}{8}\cdot U\cdot|U|\cdot\frac{P}{A}=0 \quad (8)$$

Dynamic ventilation experiments and validation of the ODE-based airflow model. Dynamic ventilation experiments were conducted to collecting data for validating the ODE-based airflow model under dynamic boundary conditions. As shown in Table 1, tests were conducted with dynamic ventilation power at 3 constant water flow rates, and with dynamic water flow rate at 7 ventilation power levels. With each constant water flowrate, the power provided to the air pump was adjusted slowly between 0.6 and 1.8 hp with an increment of 0.01 hp per 30 s, and rapidly between 0.6 and 2 hp with an increment of 0.1–1.2 hp per 15 s - 2 min. In tests with dynamic water flows, the water flow was switched between 142 and 405 L/min. During all tests, the velocity sensors were fixed at half the headspace height (average headspace height was used when the water level was dynamic).

The Saint-Venant equations were implemented (with n determined above) to predict the water depth and velocity. The ODE-based airflow model was implemented for the pilot sewer section between the air pressure sensors to predict air velocity according to measured pressure data, with the *Cd* and *f* values calibrated above. The model-predicted air velocity was compared with the measured air velocity, with the *RMSE*, *MRE*, and R^2 calculated as the performance indicators.

3.2. Desktop simulation to evaluate the model performance in network modelling

Simulated network. Desktop simulation studies in both forced and natural ventilation conditions were conducted to evaluate the performance of the proposed ODE-based model in a hypothetical sewer network (network A) with 18 pipes and 12 access chambers (Fig. 3).

Boundary conditions. There are 7 air pressure boundaries (p_1- p_7) and 6 water flowrate boundaries (Q_{w1}- Q_{w6}). The water flow rates applied to the main sewer line (Q_{w6}), and the side sewer lines (Q_{w1}- Q_{w5}) were typical water flow profiles measured at two real sewer pipes of similar sizes, as displayed in Figure S6 in part S10 of SI. The cross-sectional areas of the water inflow boundaries were calculated using the Manning's equation, which was helpful to reduce numerical oscillations and improve the stability and efficiency of the airflow model.

In the simulation of natural ventilation, the atmospheric pressure measured at a real sewer site on October 8th, 2023 was used as the boundary pressure p_7 (Figure S7 in part S10 of SI). Other boundary pressures p_1 - p_6 were assigned as according to Eq. (9), so that the pressure difference between p_i ($i = 1, 2, \ldots, 6$) and p_7 completely offsets the gravity of air. This means, if there is no water flow or forced ventilation, air movement inside the pipes would not occur.

$$p_i = p_7 + (h_7 - h_i)\cdot g\cdot p_7/(287.058\cdot T) \quad (9)$$

where h_i ($i = 1, 2, \ldots, 6$) refers to the elevation of the pipe inverts at the i^{th} boundary; h_7 is the elevation of the pipe invert at the 7th boundary.

For the simulation of forced ventilation, the ventilator at boundary 1 is assumed to impose an additional negative pressure that stepwise changed between 0 and −24 Pa, as shown in Figure S8 (part S10 of SI), to mimic different levels of ventilation. p_2 - p_7 were set as described in the natural ventilation simulation.

To assess the efficiency of the ODE-based airflow model with larger networks, we conducted simulation of a more complex real-world sewer

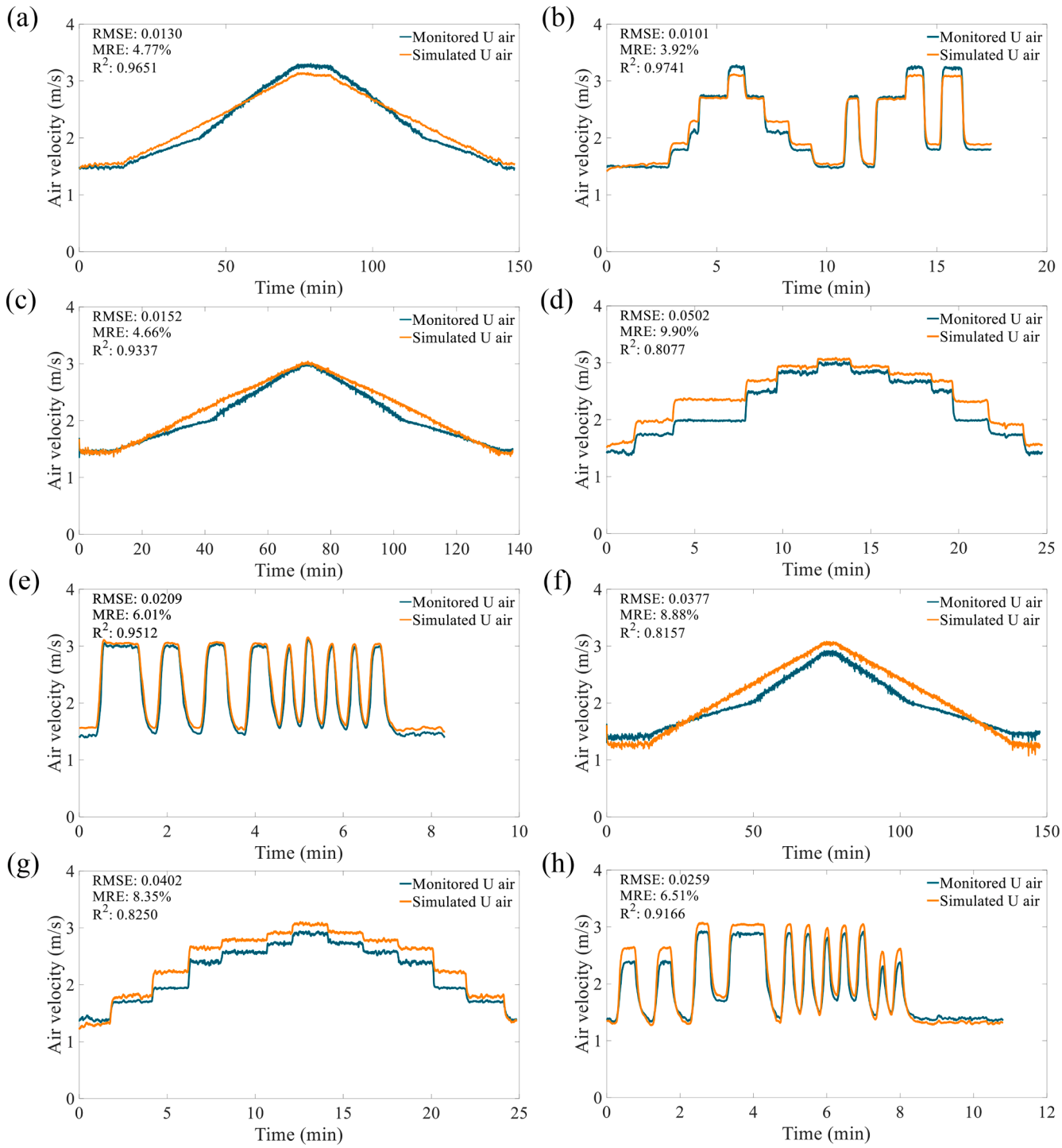

Fig. 5. Measured and simulated air velocity profiles in the third set of experiments with constant water flowrates of 285 L/min (a-b), 523 L/min (c-e), 775 L/min (f-h).

system (network B) comprising 145 pipes and 146 access chambers (part S15 of SI). The computational time was recorded and compared with that for network A.

The simulation was performed on a desktop computer with an 11th Gen Intel (R) Core (TM) i7–11700 @ 2.50 GHz CPU and 32 GB of RAM.

4. Results

Calibration of *n*, C_d and *f*. Based on the hydraulic characteristics in the first set of experiments, the Reynolds numbers were calculated (Table S4 in part S11 of SI), which indicate the water flows in all experiments were turbulent. The *n* value was calibrated to be 0.0089 ± 0.0002, which falls in the general range of Manning's coefficient of PVC pipes (0.009 - 0.011). The fit between the model-predicted and the experimentally determined water velocity shown in Figure 4(a) are acceptable. The hydraulic model overestimated the water flow velocities at lower water velocities. Sediments/biofilms were visibly present at the lower part of the pipe, which likely increased the frictional resistance with a more pronounced effect when the water depth was lower.

In the second set of experiments, the measured air pressure and air

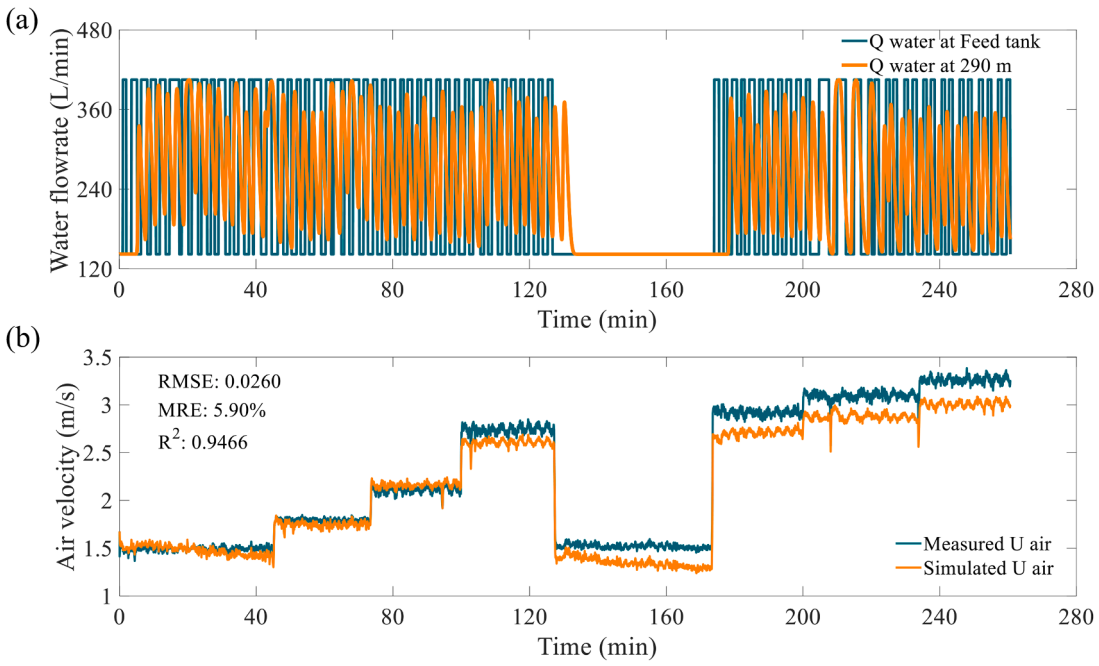

Fig. 6. The pumped water flowrate and simulated water flowrate at 290 m (a), and measured and simulated air velocities (b) in the experiment with dynamic water flow.

velocity data (shown in Figure S9 and S10 in part S12 in SI) were used to calibrate the C_d (0.0208 ± 0.0011) and f (0.0204 ± 0.0004) values, which fall in the respective ranges reported (Qian et al., 2021). The predicted air velocities obtained by solving Eq. (8) using the measured air pressure and the calibrated C_d and f, are compared with the measured air velocities in Fig. 4(b). The *RMSE*, *MRE*, R^2 values demonstrate the goodness of the fitting of parameter C_d and f and the effectiveness of prediction of the air velocity using these calibrated parameters in steady state condition. The model appears to underestimate the air velocity when the latter was lower than 1.5 m/s. This might have been caused by measurement errors, but more fundamental reasons (e.g. f is no longer constant at lower air velocities) cannot be excluded.

Model validation. With the measured pressures in the third set of experiments (with dynamic ventilation) as the boundary conditions, the developed ODE-based airflow model (Eq. (6)) was used to predict the air velocities. The simulated air velocity profiles in scenarios with constant water flowrates are compared with the measured air velocities in Fig. 5. In the scenario with dynamic water flows, the water cross-section area and velocity along the pipe were obtained using the hydraulic model with the calibrated n (see Fig. 6(a) for water flow rate), and were provided to the ODE-based airflow model (Eq. (6)) as inputs. The simulated and measured air velocity profiles are compared in Fig. 6(b).

In all cases, the simplified model satisfactorily predicted the dynamic trend of air velocities, demonstrating the robustness of the dynamic model. The mean relative errors were between 3.3 % and 10 %, which is considered acceptable, considering the quality of the online sensors. The model slightly underestimated the air velocity in the cases where the water flowrate was high. It is possible that the friction between water and air increases at a higher water flow rate due to a rougher water surface. This could be addressed in future studies by modelling C_d as a function of the water velocity.

Model performance evaluation. The simulated air velocity profiles at multiple locations in the simulated network A, with the full, PDE-based and the simplified, ODE–based airflow models, are compared in Fig. 7. In both the natural and forced ventilation scenarios, the RMSE and R^2 values show that the results of the two models are highly consistent, demonstrating that the ODE-based model can be used to replace the PDE-based model for airflow modelling in sewer networks. Compared to the PDE-based model, the simplified model increases the simulation speed by two orders of magnitude, as shown in Table S5 in part S13 of SI.

The total number of pipes and nodes in network B is nearly ten times that in network A. The ODE-based model also successfully predicted air velocities across the network B under various ventilation conditions (examples are presented in Figure S16 in part S15 of SI), with a simulation time (17.3 h) less than ten times that for network A (1.9 – 2.1 h), on the same computer and for the same simulated time of one day (Table S5 in part S13 of SI). This indicates that the computational time of the ODE-based model increases approximately linearly with the size of the network, and the network size should guide the choice of computing resources.

5. Discussion

Airflow models are important in ventilation design for corrosion and odour management. Current models are either overly complicated thus computationally demanding (i.e. PDE models), or overly simplistic ignoring airflow dynamics (steady-state models) or sacrificing accuracy (empirical models). Steady-state models possess excellent computational speed for simulations in large-scale networks but are only suitable for steady state scenarios. However, sewer networks are truly dynamic systems with hydraulic and pressure conditions varying over time. Most empirical models simply connect airflow rate with water velocity and sewer morphology and do not even conserve masses.

In this study, we numerically solved the PDE-based 1D full model (i.e. the NSE), along with the Saint-Venant Equations for sewer hydraulics, with a range of pipe geometries, water flow rates and pressure boundary conditions, and analysed the simulation results. The air velocity is approximately uniform across the entire pipe in all simulated scenarios, which had not been discovered in previous studies according to the best of our knowledge. In contrast, the air pressure is not uniform but varies approximately linearly along the pipe, which overcomes the friction forces and induces approximately equal acceleration of air at all locations. This ensures uniform air velocity along the pipe. These observations remain true even with complex and rapidly changing pressure conditions at boundaries, providing us with a foundation to simplify the

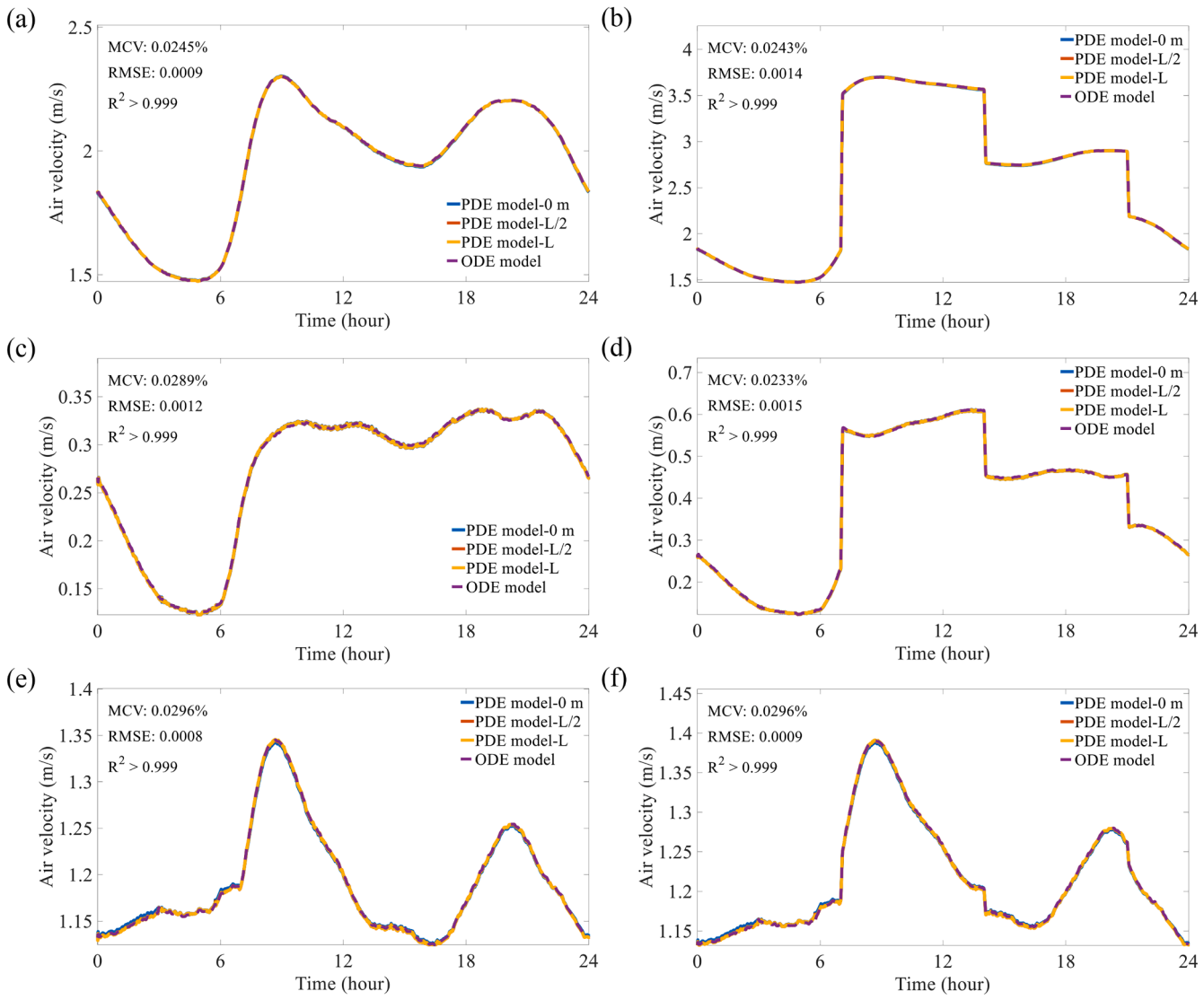

Fig. 7. Comparison of the full and simplified models when applied to airflow modelling in sewer network A with natural (a, c, e) and forced ventilation (b, d, f). Pipes 1, 9,18 are shown here as examples (see Figure S11-S12 in part S14 of SI for all locations).

airflow model to a single ODE for the whole pipe. This means that the air velocity in each pipe can be obtained by solving a single ODE (i.e. the spatial discretisation along the pipe is no longer needed). This was verified with data collected from a pilot sewer pipe (300 m in length and 0.238 m in diameter) via a comprehensive experimental program. A single ODE, following the calibration of its parameters C_d and f, was able to reproduce the air flow and velocity data across the pipe.

The developed 1D ODE-based simplified model in this study has a high-level fidelity with the full PDE-based model, but is much faster. It can be used in network-scale air velocity and pressure simulations, thus providing necessary information for ventilation design and comprehensive modelling of sewer networks including H_2S, moisture, and temperature modelling in support of corrosion prediction and mitigation.

The simplified airflow model can be integrated with the sewer hydraulic and process models to form an efficient and powerful tool for sewer corrosion and odour management. The sewer hydraulic processes should be run prior to other models. This is because the in-sewer hydraulic processes are not significantly influenced by the airflows or the in-sewer chemical or biological reactions. The airflow model should be run subsequently with the hydraulic model outputs as its inputs. Alternatively, the airflow model could be solved simultaneously with hydraulic model, with real-time import of simulation data form the hydraulic model as its input. Finally, the process models describing the in-sewer chemical, biological and mass and heat transfer processes (Zhang et al., 2023; Li et al., 2023) can be solved as the last step with the predictions by both the hydraulic and airflow models as their inputs. Thus, the development of the simplified, ODE-based airflow model in this work makes the effective and efficient integration of all these models possible, providing strong support to science-based corrosion and odour management. At present, these models have not been implemented in a single commercial modelling platform. End users need to undertake these steps using separate modelling packages and manually transfer data between these packages. The developed airflow model can be implemented in any platform with ODE solvers.

6. Conclusions

The airflow in a sewer pipe can be adequately modelled using an ordinary differential equation. The ODE-based model derived in this study has a high-level fidelity with the full one-dimensional Navier-Stokes equations, and could well describe the experimental data collected from a pilot sewer pipe under a variety of water flow and ventilation conditions. Due to much reduced complexity compared to

the Navier-Stokes equations, which require solving partial differential equations, the ODE-based airflow model is computationally much more efficient, improving the simulation speed by approximately two orders of magnitude. The proposed airflow model can be integrated with sewer hydraulic and process models to provide strong support to sewer odour and corrosion management.

CRediT authorship contribution statement

Tao Shi: Writing – original draft, Visualization, Validation, Methodology, Investigation, Formal analysis, Data curation, Conceptualization. **Jiuling Li:** Writing – review & editing, Supervision, Project administration, Methodology, Funding acquisition, Formal analysis, Conceptualization. **Jingyu Ge:** Writing – review & editing, Visualization, Methodology. **Shane Watts:** Resources, Investigation. **Yaran Wang:** Methodology, Conceptualization. **Keshab Sharma:** Writing – review & editing, Supervision, Project administration, Conceptualization. **Zhiguo Yuan:** Writing – review & editing, Visualization, Supervision, Project administration, Methodology, Funding acquisition, Formal analysis, Conceptualization.

Declaration of competing interest

The authors declare that they have no known competing financial interests or personal relationships that could have appeared to influence the work reported in this paper.

Acknowledgements

The authors acknowledge the Reducing Sewer Corrosion through Model-supported Ventilation Control Project LP190101262, jointly funded by the Australian Research Council (ARC), Urban Utilities, Water Corporation, Melbourne Water, and DC Water. The authors are grateful to Urban Utilities, for support of the site for pilot sewer experiments. Tao Shi thanks the China Scholarship Council for Scholarship Support. Zhiguo Yuan is a Global STEM Professor jointly funded by the Innovation, Technology and Industry Bureau ("ITIB") and Education Bureau ("EDB") of the Government of the Hong Kong Special Administrative Region, China and acknowledges financial support from the Hong Kong Jockey Club Charities Trust for the JC STEM Lab of Sustainable Urban Water Management.

Supplementary materials

Supplementary material associated with this article can be found, in the online version, at doi:10.1016/j.watres.2024.123083.

Data availability

Data will be made available on request.

References

Brown, R.F., 1937. North outfall sewer inspection, city of Los Angeles. Sewage Work J 9 (3), 446–454.
Bu, H., Carvalho, G., Yuan, Z., Bond, P., Jiang, G., 2021. Biotrickling filter for the removal of volatile sulfur compounds from sewers: a review. Chemosphere 277, 130333.
Capart, H., Sillen, X., Zech, Y., 1997. Numerical and experimental water transients in sewer pipes. J. hydraulic res. 35 (5), 659–672.
Corsi, R.L., Chang, D. and Schroeder, E. 1989. Assessment of the effect of ventilation rates on VOC emissions from sewers 31(7), 147–157.
Donaldson, D., 1932. Sewer ventilation, why and how? Sewage Work J 4 (1), 108–113.
Durrenmatt, D.J., Wanner, O., 2014. A mathematical model to predict the effect of heat recovery on the wastewater temperature in sewers. Water Res. 48, 548–558.
Edwini-Bonsu, S., Steffler, P.M., 2004. Air flow in sanitary sewer conduits due to wastewater drag: a computational fluid dynamics approach. J Environm/Eng. Sci. 3 (5), 331–342.
Edwini-Bonsu, S., 2006a. Dynamics of Air Flow in Sewer Conduit Headspace. J, Hydraulic Eng. 132 (8), 791–799.
Edwini-Bonsu, S., 2006b. Modeling Ventilation Phenomenon in sanitary sewer systems: a system theoretic Approach. Journal of Hydraulic engineering 132 (8), 778–790.
Figueroa, A., Hadengue, B., Leitao, J.P., Rieckermann, J., Blumensaat, F., 2021. A distributed heat transfer model for thermal-hydraulic analyses in sewer networks. Water Res. 204, 117649.
H., L.C, 1965. Sewer corrosion potential. Water Poll.Control Feder. 37 (8), 1067–1091.
Hurse, T.J., Ochre, P., 2008. The lost art of sewer ventilation. J.Australian Water Associ. 35 (3), 94–98.
Jiang, G., Sun, X., Keller, J., Bond, P.L., 2015. Identification of controlling factors for the initiation of corrosion of fresh concrete sewers. Water Res. 80, 30–40.
Jiang, G., Melder, D., Keller, J., Yuan, Z., 2017. Odor emissions from domestic wastewater: a review. Crit Rev Environ Sci Technol 47 (17), 1581–1611.
Joseph, A.P., Keller, J., Bustamante, H., Bond, P.L., 2012. Surface neutralization and H2S oxidation at early stages of sewer corrosion: influence of temperature, relative humidity and H2S concentration. Water Res. 46 (13), 4235–4245.
Li, J., Sharma, K., Li, W., Yuan, Z., 2022. Swift hydraulic models for real-time control applications in sewer networks. Water Res. 213, 118141.
Li, J., Mohamad, N.N.N., Sharma, K., Yuan, Z., 2023. Establishing boundary conditions in sewer pipe/soil heat transfer modelling using physics-informed learning. Water Res. 244, 120441.
Liang, Z., Xie, W., Li, H., Li, Y., Jiang, F., 2024. Integrating machine learning algorithm with sewer process model to realize swift prediction and real-time control of H2S pollution in sewer systems. Water Res. X 23, 100230.
Lowe, S., 2017. Sewer ventilation modeling. Journal of Water Management Modeling 25 (C415), 1–8.
Matos, R.V., Ferreira, F., Gil, C., Matos, J.S., 2019a. Understanding the effect of ventilation, intermittent pumping and seasonality in hydrogen sulfide and methane concentrations in a coastal sewerage system. Environ. Sci. Pollut. Research 26 (4), 3404–3414.
Matos, R.V., Ferreira, F., Matos, J.S., 2020. Influence of ventilation in H_2S exposure and emissions from a gravity sewer. Water Sci. Technol. 81 (10), 2043–2056.
Pomeroy, R., 1945. The pros and cons of sewer ventilation. Sewage Work J 17 (2), 203–208.
Pomeroy, R., Bowlus, F.D., 1946. Progress report on sulfide control research. Sewage Work J 18 (4), 597–640.
Qian, Y., Zhu, D.Z., Edwini-Bonsu, S., 2018. Air flow modeling in a prototype sanitary sewer system. J. Environ. Eng. 144 (3), 04018008.
Qian, Y., Shao, W., Zhu, D.Z., Mohamad, K.A.A., Steffler, P.M., Edwini-Bonsu, S., Yue, D., Krywiak, D., 2021. Modeling air flow in sanitary sewer systems: a review. J. Hydroenviron. Res. 38, 84–95.
Song, Y., Wightman, E., Kulandaivelu, J., Bu, H., Wang, Z., Yuan, Z., Jiang, G., 2020. Rebar corrosion and its interaction with concrete degradation in reinforced concrete sewers. Water Res. 182, 115961.
Song, Y., Chetty, K., Garbe, U., Wei, J., Bu, H., O'Moore, L., Li, X., Yuan, Z., McCarthy, T., Jiang, G., 2021. A novel granular sludge-based and highly corrosion-resistant bioconcrete in sewers. Sci. total environment 791, 148270.
Studley, E.G., 1939. Experimental ventilation of the north outfall sewer of the city of Los Angeles. Sewage Work J 11 (2), 264–270.
Thistlethwayte, D.K.B., 1972. The Control of Sulphides in Sewerage Systems. Butterworths, Sydney.
Vollertsen, J., Nielsen, A.H., Jensen, H.S., Wium-Andersen, T., Hvitved-Jacobsen, T., 2008. Corrosion of concrete sewers - the kinetics of hydrogen sulfide oxidation. Sci. total environ. 394 (1), 162–170.
Wang, Y.C., Nobi, N., Nguyen, T., Vorreiter, L., 2012. A dynamic ventilation model for gravity sewer networks. Water Sci. Technol. 65 (1), 60–68.
Ward, M., Hamer, G., McDonald, A., Witherspoon, J., Loh, E., Parker, W., 2011. A sewer ventilation model applying conservation of momentum. Water Sci. Technol. 64 (6), 1374–1382.
Zhang, L., Qiu, Y.Y., Sharma, K.R., Shi, T., Song, Y., Sun, J., Liang, Z., Yuan, Z., Jiang, F., 2023. Hydrogen sulfide control in sewer systems: a critical review of recent progress. Water Res. 240, 120046.
Zhang, Q., Shao, W., Zhu, D.Z., Xu, W., 2020. Steady air flow model for large sewer networks: a theoretical framework. Water Sci. Technol. 82 (3), 503–512.
Zobeyer, H., Zhu, D.Z., Edwini-Bonsu, S., 2020. Air flow model development and application in a complex combined sewer system. Water Sci. Technol. 82 (8), 1687–1700.
Zuo, Z., Xing, Y., Lu, X., Liu, T., Zheng, M., Guo, M., Liu, Y., Huang, X., 2024. Nitrite-dependent microbial utilization for simultaneous removal of sulfide and methane in sewers. Water Res. X 24, 100231.